PAPER

Check for updates

Effects of Co/Ce molar ratio and operating temperature on nanocatalyst performance in the Fischer–Tropsch synthesis†

Tahereh Taherzadeh Lari, [iD] *[a] Ali Akbar Mirzaei[a] and Hossein Atashi[b]

Iron–cobalt–cerium three-metal nanoparticles have been obtained by a solvothermal method for converting synthesis gas into light olefins. The effect of various fabrication molar ratios of Co/Ce and the effect of the operating temperature (270–400 °C) on the activity and selectivity were demonstrated. The nanocatalyst with a 1 : 1/4 Co/Ce molar ratio at an operating temperature of 300 °C performed optimally in selectivity converting synthesis gas into light olefin. The nanocatalysts prepared with different Co/Ce molar ratios were characterized. The morphology, structure and magnetic behavior were established by SEM, EDX, FTIR, XRD and VSM *techniques.

1. Introduction

Fischer–Tropsch FT synthesis is a significant gas-to-liquid process by using a metal catalyst for the conversion of synthesis gas (CO + H$_2$) derived from coal, natural gas or biomass into hydrocarbons and oxygenated compounds. FT synthesis produces a wide range of olefins, paraffin and oxygenated products (such as alcohols, aldehydes, acids and ketones). The main concerns with the Fischer–Tropsch FT synthesis are in increasing environmental requests, technological developments and changes in fossil energy. This resources have been used exclusively for hydrocarbon selectivity towards light olefins including ethylene, propylene, butylene (C$''_2$–C$''_4$), which are the petrochemical feedstock.[1,2] Among the variables that influence the spread of the products, the effects of the catalyst molar ratio and operating temperature are prominent factors affecting the hydrocarbon product selectivity.[3] An increase in the temperature causes selective methane formation, and deposition of carbon, and thereby catalyst deactivation and a shorter average length of product. With increasing temperature, the selectivity changes to mainly methane at a higher cobalt molar ratio; whereas, reversely, for iron, methane selectivity remains low even at high temperature. On the other hand, comparatively, as the cobalt volume increases, the iron produces more methane and less olefin and the effect of pressure on the catalyst with higher amounts of cobalt becomes more prominent, while for the catalyst with a higher iron molar ratio, the pressure has little effect on the product selectivity. The effect of total pressure can be described by the CO partial pressure, which results in a lighter-hydrocarbon selectivity and H$_2$ partial pressure that causes paraffin's product selectivity. For cobalt catalysts, as the pressure increases, the wax selectivity increases.[4,5] Among the group (VIII) transition metals, only Fe, Ni, Co and Ru have the required Fischer–Tropsch reaction properties. Until today, both iron and cobalt are the only elements used as catalysts for industrial applications.[6] Iron and cobalt are the catalysts of choice for industrial applications; iron is inexpensive and is tolerated, flexible and works under operational conditions that give a broad product range. Cobalt-based catalysts are much more expensive than iron-based ones. Co-Based catalysts with longer lifetimes have a higher hydrogenation activity. Therefore, they tend to produce a higher efficiency with the heavier paraffin's molecular weight and many fewer oxygenates, when compared to the iron catalyst.[7] It is worth studying ceria addition as a promoter for Fe–Co catalysts because of its controversial role. This is related to the function of CeO$_2$ on catalyst activity, which can result in either higher or lower C$''_2$–C$''_4$ selectivity.[8] Moreover, the iron–cobalt–cerium catalyst has a beneficial application in the industry and it is distinguishable that a higher selectivity can be obtained on Fe–Co–Ce catalysts than other iron or cobalt based catalysts. There have been several published studies on Co–Ce and Fe–Co binary catalysts. Further studies demonstrate the following conclusions: the catalyst containing 80% of Co and 20% of Ce performed optimally for the conversion of synthesis gas into light olefins.[9] The effect of the procedural conditions on the Fe–Co–Mn supported by MgO was studied.[10] Despite the wide range of applications for iron–cobalt binary oxide nanoparticles, there is no study on iron–cobalt–cerium ternary oxides.

[a]Department of Chemistry, Faculty of Science, University of Sistan and Baluchestan, P. O. Box 98135-674, Zahedan, Iran. E-mail: tzd.tahereh@yahoo.com; Taherzadeh@pgs. usb.ac.ir; Tel: +98 9173613223

[b]Department of Chemical Engineering, Faculty of Engineering, University of Sistan and Baluchestan, P. O. Box 98164-161, Zahedan, Iran

† Electronic supplementary information (ESI) available. See DOI: 10.1039/c7ra05490d

In the present study, we probe the effects of various preparation molar ratios of Co/Ce, as well as the influences of different operational temperatures on iron–cobalt with cerium rare earth nanocatalysts in a fixed-bed reactor (FBR), so that synthesis gas conversion into light olefins could be evaluated. The comparison of catalytic activities and selectivities of each catalyst is discussed. The catalysts with the optimized molar ratios of cerium that have both high activities and valuable olefin selectivity are also presented. In addition, several techniques have been used including SEM, EDS, XRD, FTIR for morphology and structural properties and physicochemical properties such as TPR for reducibility and VSM for magnetic behavior of three metals prepared *via* solvothermal method.

2. Experimental

2.1. Materials

All the chemicals were of analytical grade and used without further purification. Iron nitrate(II) nonahydrate (Fe(NO$_3$)$_3$·9H$_2$O, 99%), cobalt nitrate(II) hexahydrate (Co(NO$_3$)$_2$·6H$_2$O, 99%), cerium nitrate(III) hexahydrate (Ce(NO$_3$)$_3$·6H$_2$O, 99%), toluene (C$_7$H$_8$, 99%), and ethanol (C$_2$H$_5$OH, 99%) were purchased from Merck. Oleylamine (C$_{18}$H$_{37}$N, 70%) was purchased from Aldrich.

2.2. Nanocatalyst synthesis and description

The iron–cobalt–cerium three-metal nanocatalysts were synthesized using a typical solvothermal method. The preparation method can be described as how different amounts of cerium and cobalt perform, as follows: 0.5, 0.25 and 0.125 g (1.1, 0.5 and 0.25 mmol) of cerium nitrate, 0.32, 0.16 and 0.08 g (1.1, 0.5 and 0.25 mmol) of cobalt nitrate, and 0.38 g (1.1 mmol) of iron nitrate were added into 50 mL of toluene containing 5.4 g (20.2 mmol) of oleylamine. The useful volume of the plastic container of the autoclave is 55 cm^3; we used 80% of useful volume, which is 44 cm^3. Therefore, the total volume of used liquid (mL of solvent + oleylamine = B + C) and solid (g of nitrate salts = A) is 44 cm^3. If the grams of nitrate salts = A, (44 cm^3 − A = F) then F is the volume of solvent + oleylamine; with knowing the volume of oleylamine, the volume of the required solvent is achieved. The mixture solution was subsequently transferred into an 80 mL Teflon-lined autoclave and heated to 180 °C. The autoclave was sealed and maintained at the given temperature for 18 h before it was allowed to cool down to room temperature. The nanoparticles formed were precipitated in the excess ethanol and further isolated from each other by centrifugation. The resulting nanoparticles were finally transferred to an oven to be dried before calcination at 100 and 500 °C in air for 4 h.

2.3. Characterization

2.3.1. X-ray diffraction XRD. X-ray diffraction (XRD) patterns of iron–cobalt–cerium three-metal nanocatalysts were recorded in the range of 10–110° (2θ) at room temperature (2θ step = 0.020 with a counting time of 0.35 s per step) using an EXPERT PHILIPS X-ray diffraction system equipped with a Cu

Kα radiation source (λ = 1.54046 Å) operated at 40 kV and 30 mA. The data were refined using the Xpert software. The XRD measurement error coefficient was 10%. The average diameter of the nanocrystalline domain was determined from the full width at half-maximum (fwhm) of the strongest reflection peak (111 reflection) using Scherrer's equation:

$$D = \frac{K\lambda}{\beta \cos \theta}, \tag{1}$$

where D denotes the mean particle size; λ, the X-ray wavelength; β, total width at half maximum; and θ, the diffraction angle.

2.3.2. Fourier transform infrared spectroscopy FTIR. FTIR spectra were collected in the region from 400–4000 cm^{-1} using a PerkinElmer Spectrum TWO spectrophotometer. The nanoparticles were analyzed by dispersing powders in KBr pellets.

2.3.3. Temperature-programmed reduction TPR. Different mixed oxide samples were subjected to temperature-programmed reduction (TPR) with hydrogen using an automated nanoparticle characterization system, which incorporated a thermal conductivity detector (TCD). The sample (0.05 g) was loaded into the quartz TPR cell and the experiments were carried out at a heating rate of 5 °C min^{-1}. The reactive gas composition was H$_2$ (5 vol%) in argon. The flow rate was fixed at 20 mL min^{-1} (STP). The total reactive gas consumption was measured during a TPR analysis. TPR measurements were carried out following activation after cooling the sample to 40 °C in an argon flow. The sample was then maintained at 50 °C under the argon flow in order to remove the remaining adsorbed oxygen until the TCD signal returned to the baseline. Subsequently, the TPR experiments were performed up to a temperature of 850 °C.

2.3.4. Scanning electron microscopy SEM. The morphology of samples was determined using a scanning electron microscope (SEM MIRA II LMU/TESCAN EDS) with an accelerating voltage of 1500 kV. For SEM analysis, the sample in ethanol was dispersed on an aluminum foil wrapped on the aluminum stub used for sample mounting. The samples were dried in air and the stub was mounted in the SEM chamber. The particle size was measured at a resolution of 200 nm with a magnification of 15 000×.

2.3.5. Energy dispersive spectroscopy EDS. The amounts and types of iron, cobalt, and cerium elements were determined by energy dispersive X-ray (EDS) attached to the scanning electron microscope.

2.3.6. Vibrating sample magnetometer VSM. The magnetic properties of the iron–cobalt–cerium three-metal nanoparticles were studied in a vibrating sample magnetometer (magnetic analysis was taken from VSM lab of Sistan and Baluchestan University). VSM measurements were accomplished by taking 0.02 g of the solid sample on the tips of the vibrating rod and analyzing them at room temperature with a maximum magnetic field of 10 000 Oe.

2.4. Research catalytic microreactor setup

Fischer–Tropsch syntheses were performed in a stainless fixed-bed microreactor with an inner diameter of 12 mm. The catalyst

(1.0 g) was well dispersed with asbestos and loaded in the center of the reactor with the thermocouple inside. Three mass flow controllers (Model 5850E, Brooks Instrument, Hatfield, PA, USA) were used to automatically adjust the flow rate of the inlet gases containing CO, H$_2$, and N$_2$ (with 99.99% purity). A mixture of CO and H$_2$ (H$_2$/CO = 1, flow rate of each gas = 30 mL min^{-1}) was subsequently introduced into the entrance of the reactor, which was placed inside a tubular furnace (Fig. 1 and 2, Model ATU 150–15, Atbin). The reaction temperature was controlled by a digital program controller (DPC) and visually monitored by a computer through a thermocouple inserted into the catalytic bed. The catalyst *in situ* was pre-reduced under 2-bar pressure and H$_2$ flow (with a flow rate of 30 mL min^{-1}) at 400 °C for 48 h before the reaction started. In each test, 1.0 g of catalyst was loaded and all the data were collected after the time of 4 h to ensure a steady state operation was attained.

2.5. Catalytic selectivity measurement

The Fischer–Tropsch synthesis was performed with a mixture of CO and H$_2$ in the temperature range of 270–380 °C, with a H$_2$/ CO molar ratio of 1 : 1, a space velocity of 3600 h^{-1} and at 2 bar of pressure. In each experiment, for the reactor catalyst testing at each molar ratio of metals fresh catalyst was loaded to avoid a deactivation effect. An automatic backpressure regulator to adjust and modify the pressure range *via* the TESCOM software was used. Reactant and product streams were analyzed by online gas chromatography (Thermo ONIX UNICAM PROGC+) equipped with two thermal conductivity detectors (TCD) and one flame ionization detector (FID) with the ability to analyze a broad variety of gaseous hydrocarbon mixtures. One TCD was used for the analysis of hydrogen (H$_2$) and the other one was used for all the permanent gases like N$_2$, O$_2$ and CO. The analysis of hydrocarbons was done by the FID. The analysis of non-condensable gases, methane through C$_8$ hydrocarbons, was applied. The contents of the sample loop were injected automatically into an alumina capillary column. Also, helium (He) was employed as a carrier gas for the optimal sensitivity. The calibration was performed by various calibration mixtures (CH$_4$, C$_2$H$_4$, C$_2$H$_6$, C$_3$H$_6$, C$_3$H$_8$, *n*-C$_4$H$_{10}$, i-C$_4$H$_{10}$, *n*-C$_5$H$_{12}$) and pure compounds obtained from the Tarkib Gas Alvand
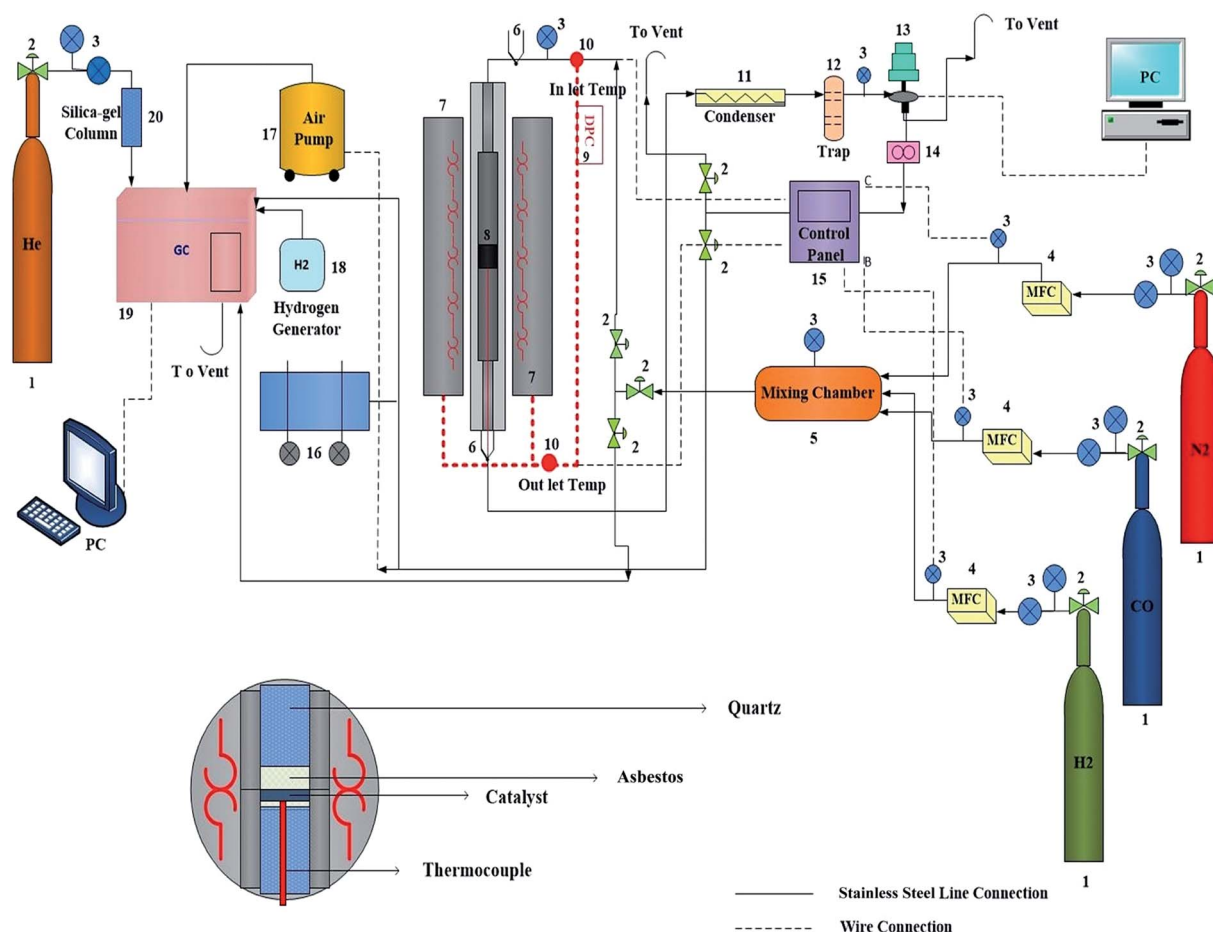

Fig. 1 Experimental setup of fixed bed reactor (FBR) for Fischer–Tropsch synthesis over iron–cobalt–cerium mixed oxide nanocatalyst: (1) gas cylinders, (2) valve, (3) pressure gauge, (4) mass flow controller (MFC), (5) mixing chamber, (6) thermocouple, (7) tubular furnace, (8) fixed bed reactor and catalyst bed (reaction zone), (9) temperature digital program controller (DPC), (10) resistance temperature detector, (11) condenser, (12) trap, (13) back pressure regulator (BPR), (14) flow meter, (15) control panel, (16) electrical motor, (17) air pump, (18) hydrogen generator, (19) gas chromatograph, (20) silica-gel column.
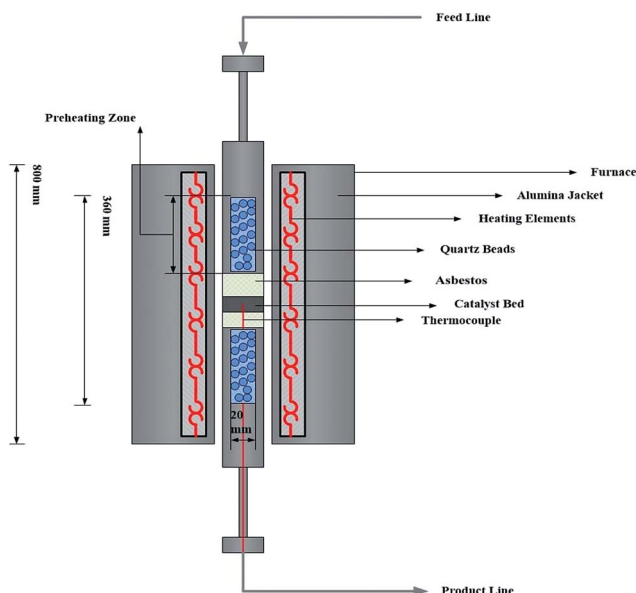
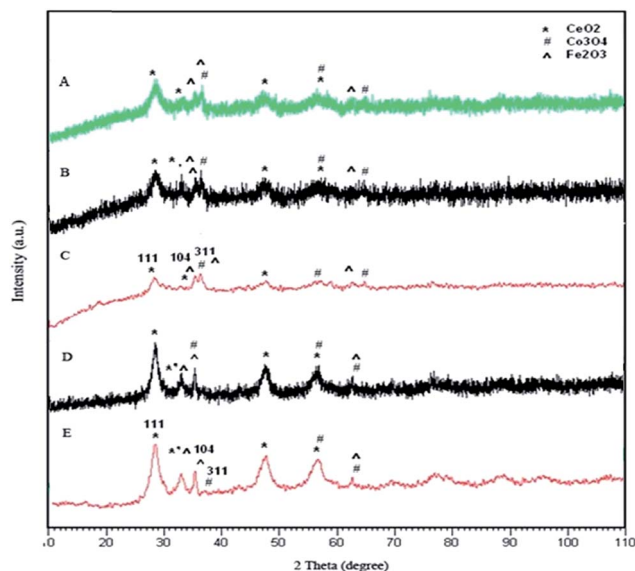Fig. 2 Schematic design of fixed-bed reactor (FBR).

Fig. 3 X-ray diffraction patterns of iron–cobalt–cerium three-metal nanocatalyst prepared at various Ce and Co molar ratios: Co/Ce: (A) 1 : 1, (B) 1 : 1/2, (C) 1 : 1/4, (D) 1/2 : 1, (E) 1/4 : 1.
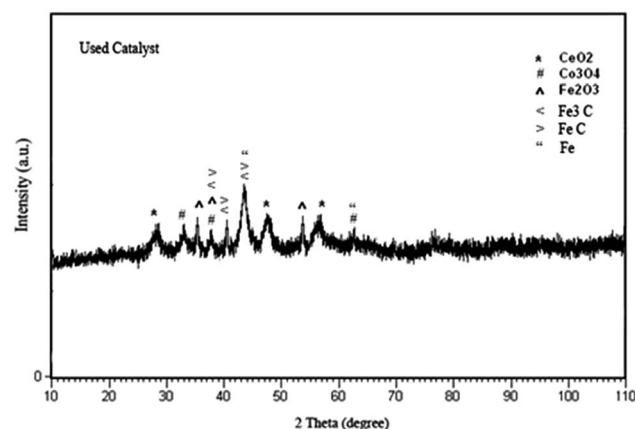
Company of Iran. The operation condition and obtained data of each experiment are presented in the ESI tables.† The CO conversion percent was calculated according to the normalization method:

$$CO \ conversion \ (\%) = \frac{(moles \ of \ CO \ in) - (moles \ of \ CO \ out)}{(moles \ of \ CO \ in)} \times 100 \quad (2)$$

3. Results and discussion

3.1. Characterization of nanocatalysts

3.1.1. Crystal structure XRD. The XRD patterns of the synthesized iron–cobalt–cerium three-metal nanocatalyst at different cerium and cobalt amounts are shown in Fig. 3. In these nanocatalysts the cubic structures of CeO_2 (card no. 34-394) and Co_3O_4 (card no. 9-418) and the rhombohedral structure of Fe_2O_3 (card no. 33-664) can be found. Here prominent Bragg reflections can be indexed as cubic and rhombohedral type structures of CeO_2, Co_3O_4, and Fe_2O_3 with the corresponding diffraction peaks of (111), (311), and (104), respectively. Meanwhile, the good crystallization of the samples and that the synthesized nanocatalysts grew more orderly in that particular direction can be proved by strong XRD reflections. Moreover, the average crystalline size of the synthesized nanocatalysts obtained by the XRD technique is estimated to be around 4.5–7.9 nm (Table S1†). The results in Table S1† show that the lower cerium amount, the higher the particle size is. The corresponding value means that a cobalt molar ratio of 1/2 is suitable to maximize the growth of iron–cobalt–cerium mixed oxides.

The XRD pattern of the used catalyst with a 1 : 1 : 1/4 of molar ratio is shown in Fig. 4. From the XRD pattern, in

Fig. 4 X-ray diffraction patterns of the used iron–cobalt–cerium three-metal nanocatalyst with the optimal 1 : 1/4 molar ratio of Co/Ce in the fixed-bed reactor.

addition to CeO_2, Co_3O_4, and Fe_2O_3, Fe_3C (card no. 23-1113), FeC (card no. 06-0686) and Fe (card no. 01-1267) were found.

3.1.2. Infrared analysis. For the nature of the oleylamine linkage in the nanocatalysts and also to characterize the surface of the iron–cobalt–cerium three-metal nanocatalysts, the FTIR spectra of the synthesized samples were recorded for various cobalt and cerium molar ratios. The resultant FTIR spectra are given in Fig. 5. The presence of a band at ~3420 cm^{-1} for all the samples shows the stretching vibration of N–H due to the absorption of the –NH$_2$ group of oleylamine on the surface of the nanocatalysts. The bands in the range of 2300–2900 cm^{-1} corresponded to the C–H stretching vibration of the oleylamine alkyl chain. The indicated vibration at 1615–1635 cm^{-1} is related to the bending vibration of the C=C group of oleylamine, which surrounds the nanocatalysts. The absorption
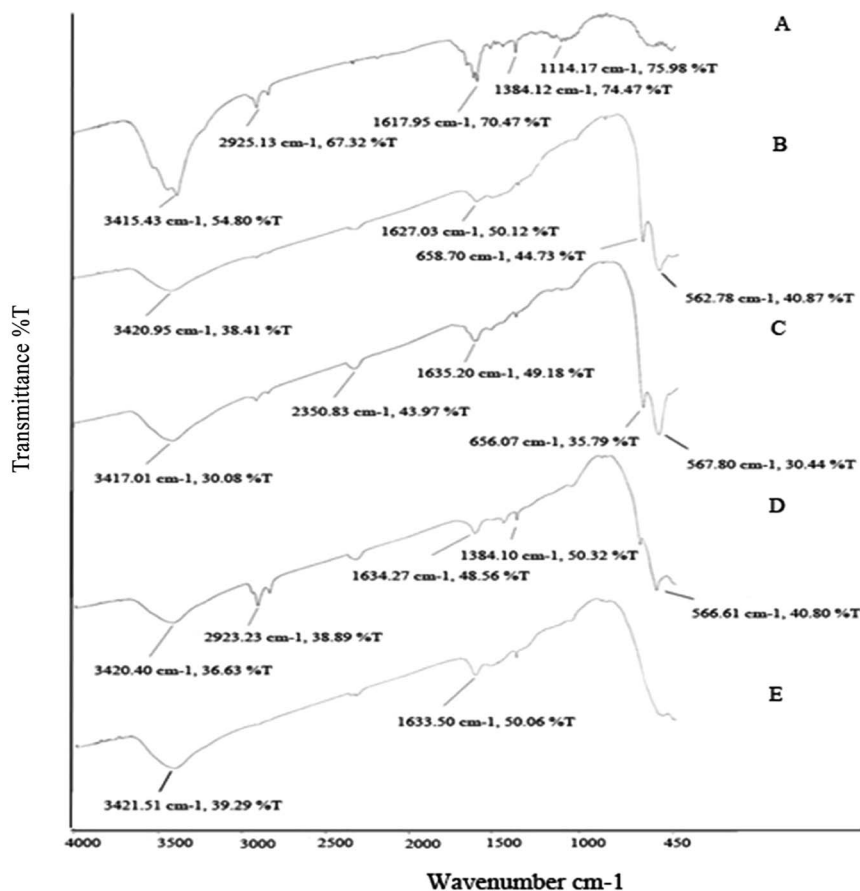
Fig. 5   FTIR spectra of iron–cobalt–cerium three-metal nanocatalysts synthesized at various Ce and Co molar ratios Co/Ce: (A) 1 : 1, (B) 1 : 1/2, (C) 1 : 1/4, (D) 1/2 : 1, (E) 1/4 : 1.

bands at 1384 cm^{-1} and 1114 cm^{-1} are assigned by the bending stretching of the $-CH_3$ group and C–H bond of oleylamine, respectively. In addition, the bands in the range of 560–660 cm^{-1} represented M–O metal ion stretching vibration.[11]

It was reported that a small change in the environment of a chemical group would lead to a change in the position of its characteristic vibrational frequencies.[12] The results indicate a relation between particle size and vibrational frequency, which by increasing the Ce molar ratio from 1/4 to 1 (decreasing the particle size) means the wave number shifts towards lower values. Whereas, by decreasing the Co molar ratio from 1 to 1/4, and thereby increasing the particle size, the wave number shifts to higher values.

3.1.3.   TPR measurements. The temperature-programmed reduction (TPR) technique was used to demonstrate the reducibility of nanocatalysts and determine the types of metal oxide species present in the synthesized samples. Hydrogen TPR profiles of nanocatalysts synthesized at various molar ratios of cerium and cobalt are indicated in Fig. 6. The phases of nanocatalysts characterized using XRD were found to be Co_3O_4 (cubic), Fe_2O_3 (rhombohedral) and CeO_2 (cubic). It has been reported that Co_3O_4 and Fe_2O_3 have two reduction peaks centered around 347 °C and 438 °C for purely cobalt oxide, while for iron oxide the first occurs at 348 °C and the second
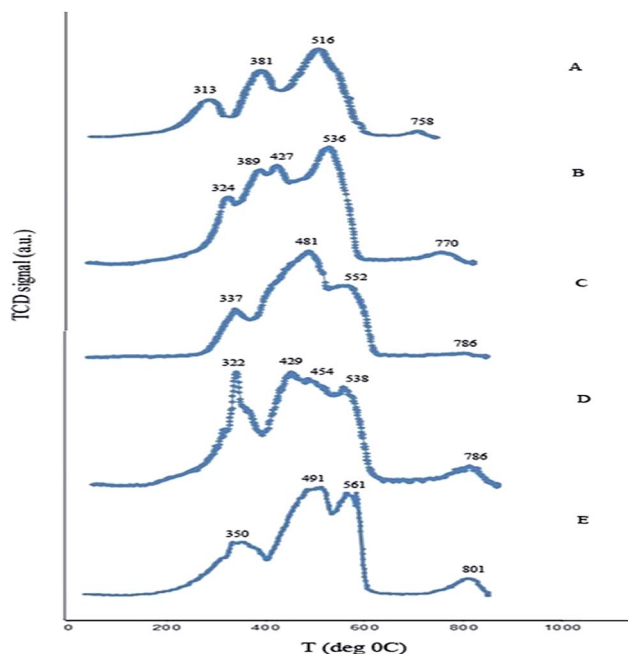

Fig. 6   TPR profiles of iron–cobalt–cerium three-metal nanocatalysts synthesized at various Ce and Co molar ratios Co/Ce: (A) 1 : 1, (B) 1 : 1/2, (C) 1 : 1/4, (D) 1/2 : 1, and (E) 1/4 : 1.

peak at 621 °C.[13,14] Also, CeO_2 indicates two peaks of hydrogen consumption centered at 485 and 800 °C.[15] For all the nano-catalysts, the TPR profiles have obvious multiple overlapping peaks resulting from different reduction steps. From Fig. 6A, the TPR profiles of the nanocatalyst with a 1 : 1 : 1 molar ratio of metals indicates four reduction peaks. The first peak, observed at 313 °C, is due to the reduction of $Fe_2O_3 \rightarrow Fe_3O_4$ and $Co_3O_4 \rightarrow CoO$. The next peak at 381 °C is attributed to the reduction of $CoO \rightarrow Co^0$ and $CeO_2 \rightarrow Ce_2O_3$. The third peak located at 516 °C is associated with the reduction of $Fe_3O_4 \rightarrow FeO \rightarrow Fe^0$. The last peak at 758 °C represents a $Ce_2O_3 \rightarrow Ce^0$ reduction. It can be seen that the reduction peaks of nanocatalysts with different amounts of cerium (Fig. 6B and C) occur at four points. The TPR profiles of iron–cobalt–cerium three-metal nanocatalysts synthesized at various cerium molar ratios of 1/2 and 1/4 are at 324, 389–427, 536, 770 and 337, 481, 552, 786 °C respectively. The first peak at 324 for the 1/2 molar ratio of cerium corresponds to the reduction of $Co_3O_4 \rightarrow CoO$ and also the peak at 337 °C for the 1/4 cerium molar ratio is associated to $Fe_2O_3 \rightarrow Fe_3O_4$ and $Co_3O_4 \rightarrow CoO$ (Fig. 6B and C). The second peak, which is divided into two peaks for the 1/2 molar ratio of cerium, represents the reduction of $Fe_2O_3 \rightarrow Fe_3O_4$ at 389 °C and the reductions of $CoO \rightarrow Co^0$ and $CeO_2 \rightarrow Ce_2O_3$ at 427 °C. Also, the sharp peak at 481 °C for the 1/4 molar ratio of cerium is related to $CoO \rightarrow Co^0$ and $Ce_2O_3 \rightarrow Ce^0$. The third peak centered at 536 and 552 °C for both the 1/2 and 1/4 cerium molar ratios is due to the reduction of $Fe_3O_4 \rightarrow FeO \rightarrow Fe^0$. The last small reduction peak at 770 and 786 °C corresponds to $Ce_2O_3 \rightarrow Ce^0$.

The TPR profiles of the nanocatalysts synthesized at various cobalt molar ratios of 1/2 and 1/4 show (Fig. 6D and E) three and four reduction peaks, respectively, positioned at 322, 429–454–538, 786 and 350, 491, 561, 801 °C. The first reduction peak centered at 322 and 350 °C is related to the reduction of both $Fe^{3+} \rightarrow Fe^{2+}$ and $Co_3O_4 \rightarrow CoO$. The second peak for the nanocatalyst with a 1/2 molar ratio of cobalt is divided into three small shoulders at 429, 454 and 538 °C, which are attributed to the reductions of $CoO \rightarrow Co^0$, $Ce^{4+} \rightarrow Ce^{3+}$ and $Fe_3O_4 \rightarrow FeO \rightarrow Fe^0$, respectively. Furthermore, the reduction peak of the nanocatalyst synthesized with a 1/4 molar ratio of cobalt centered at 491 °C is attributed to the reduction of both $CoO \rightarrow Co^0$ and $CeO_2 \rightarrow Ce_2O_3$. The third reduction peak of this sample located at 561 °C relates to the reduction of Fe_3O_4 to Fe^0. The last peak for the nanocatalysts with 1/2 and 1/4 molar ratios of cobalt centered at 786 and 801 °C corresponds to the reduction of $Ce_2O_3 \rightarrow Ce^0$.

The reduction of ceria in the presence of transition metals is easier because of a higher degree of reduction and lower temperature of reducibility. It is generally interpreted in terms of a spillover process of hydrogen from metals to ceria. In addition, a higher content of ceria leads to a higher degree of reduction by shifting towards a lower temperature. The result
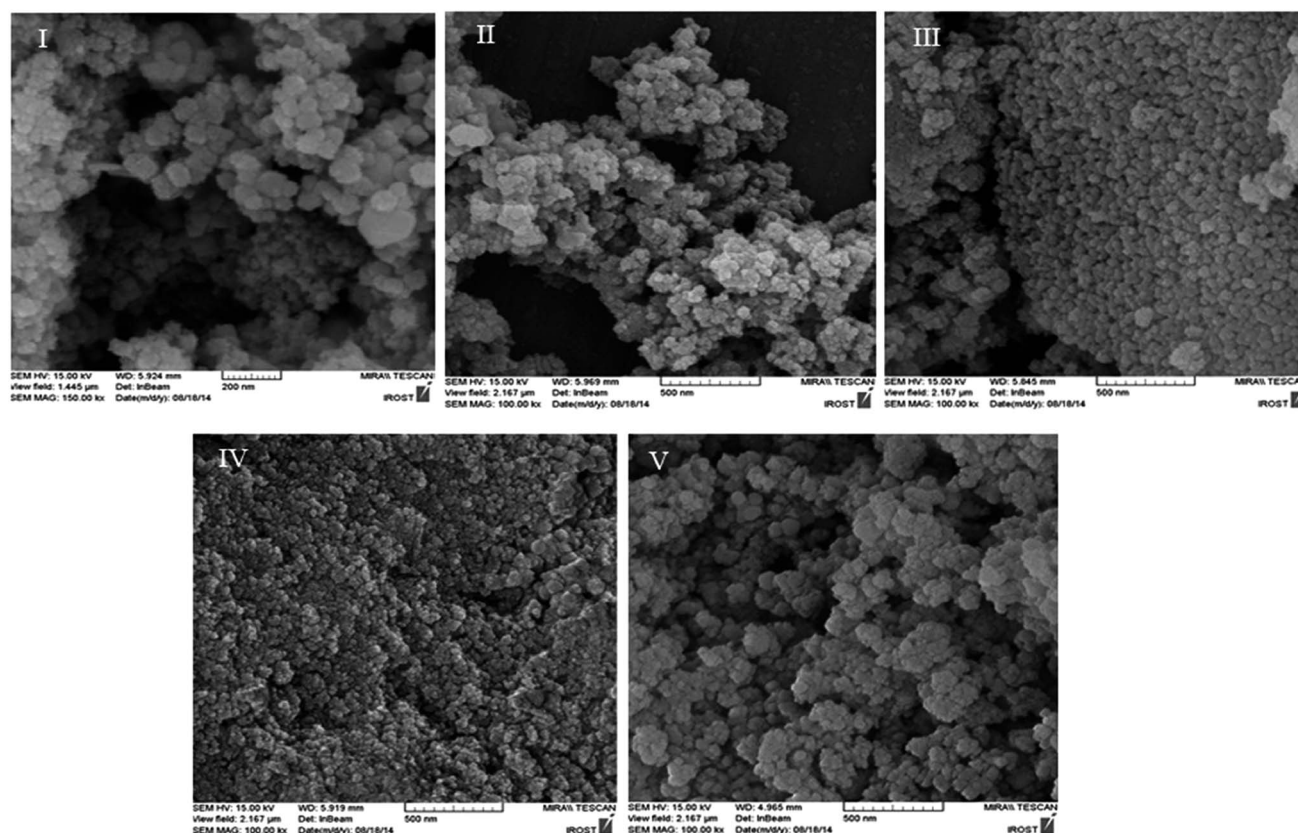

Fig. 7 SEM micrographs of iron–cobalt–cerium three metals nanocatalyst synthesized at various Co and Ce molar ratios Co/Ce: (I) 1 : 1, (II) 1 : 1/2, (III) 1 : 1/4, (IV) 1/2 : 1, (V) 1/4 : 1.

indicates that particle size is a factor affecting reducibility and causes different reduction temperatures. Therefore, by changing the cobalt and cerium molar ratio from 1 to 1/2 and 1/4, the increase in particle size leads to the reduction peaks shifting towards higher temperatures.

3.1.4. Morphology and chemical analysis. Fig. 7 indicates the SEM images for iron–cobalt–cerium three-metal nano-catalysts synthesized at various cerium and cobalt molar ratios. The SEM images display the homogeneous morphology of the nanocatalyst. In addition, the particle sizes are estimated in the range of 25–47 nm. The larger particle sizes of the nano-catalysts, as compared to the average sizes obtained from the XRD pattern (Table S$_1$†), can be associated with the existence of agglomeration caused by the effect of the stronger interaction among magnetic particles, such as van der Waals forces and magnetic dipolar interaction.[16] This reveals that the particle sizes are enhanced with reducing amounts of cobalt and cerium molar ratios.

Also, the EDS spectra of iron–cobalt–cerium three-metal nanocatalysts synthesized at various cobalt and cerium molar ratios are illustrated in Fig. 8. This indicates the presence of Fe, Co, Ce, and O (Table S$_2$† and Fig. 8), which verifies that these materials comprise oxidic phases of iron, cobalt and cerium.

3.1.5. Magnetic measurements. The magnetic properties of the synthesized iron–cobalt–cerium three-metal nanocatalysts were investigated using the VSM technique at room temperature. The effect of various cobalt and cerium molar ratios of 1, 1/2 and 1/4 on the magnetic properties of the samples was studied. The corresponding hysteresis loops are given in Fig. 9
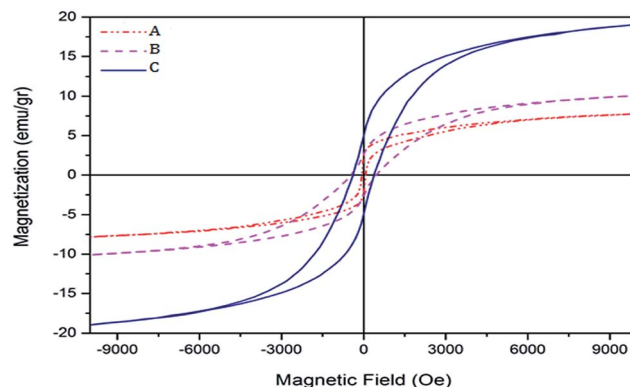

Fig. 9 Hysteresis loops of iron–cobalt–cerium three-metal nano-catalysts synthesized at various Ce molar ratios: (A) Ce = 1, (B) Ce = 1/2, (C) Ce = 1/4.

and 10, which show that all the nanocatalysts indicate ferro-magnetic behavior. The values of saturation magnetization (M_s), coercivity (H_c), residual magnetization (M_r), and residual magnetization ratio R ($R = M_r/M_s$) for variations of cobalt and cerium molar ratios are listed in Table S$_3$.† The results show that the saturation magnetization (M_s) increases by decreasing the cobalt and cerium molar ratios from 1 to 1/4 and has values between 7.768 and 11.497–19.050 emu g^{-1}, respectively, in Fig. 9 and 10. The results for nanocatalysts synthesized with various cobalt and cerium molar ratios show that the saturation magnetization increases with enhancing particle size. The saturation magnetization (M_s) and coercivity (H_c) *versus*
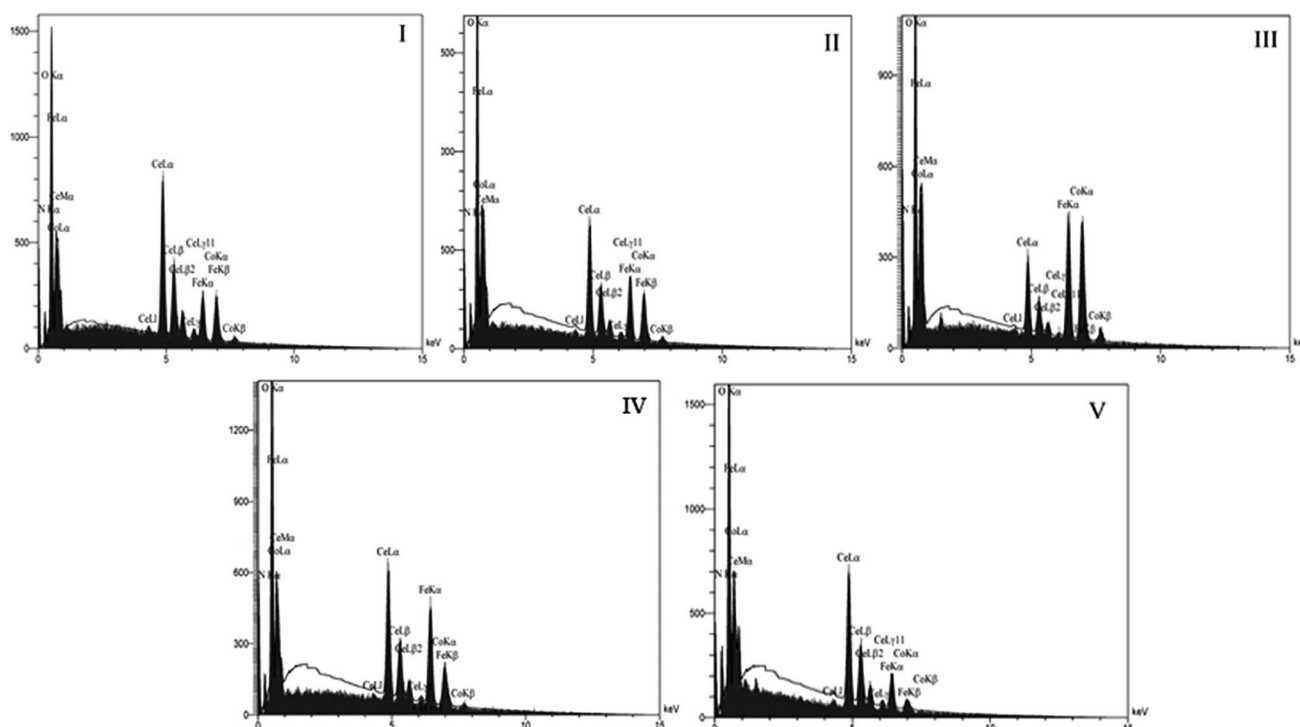

Fig. 8 EDS spectra of iron–cobalt–cerium three metals nanocatalyst synthesized at various Co and Ce molar ratios: Co/Ce: (I) 1 : 1, (II) 1 : 1/2, (III) 1 : 1/4, (IV) 1/2 : 1, (V) 1/4 : 1.
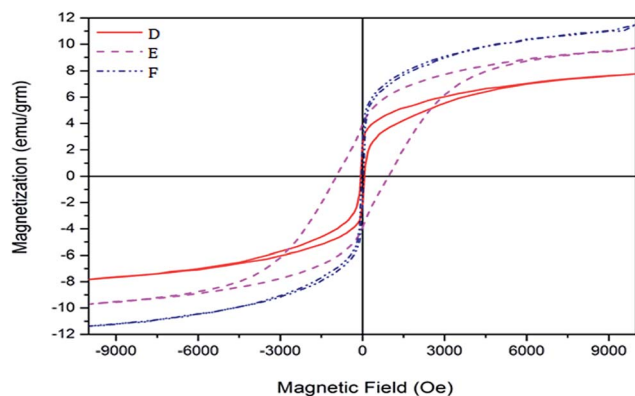
Fig. 10 Hysteresis loops of iron–cobalt–cerium three-metal nanocatalysts synthesized at various Co molar ratios: (D) Co = 1, (E) Co = 1/2, (F) Co = 1/4.
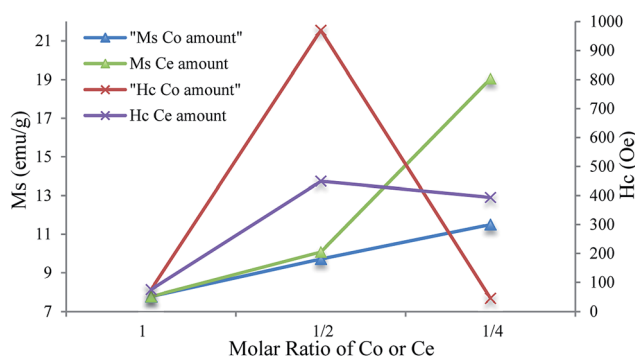

Fig. 11 Variation of saturation magnetization and coercivity of iron–cobalt–cerium three-metal nanocatalysts as a function of different molar ratios of Co and Ce.

different amounts of cobalt and cerium are shown in Fig. 11. The coercivity (H_c) and residual magnetization (M_r) for nanocatalysts synthesized with different amounts of cobalt and cerium are between 75.28 and 45.17–393.6 Oe and 2.449 and 2.831–5.018 emu g^{-1}, respectively. It was reported that $H_c < 100$ Oe is dues to a soft ferromagnetic and $H_c > 100$ Oe is due to

a hard ferromagnetic.[17] Therefore, the nanocatalysts with 1 : 1 and 1/4 : 1 molar ratios of Co/Ce have a soft ferromagnetic behavior and those prepared with 1 : 1/2, 1 : 1/4 and 1/2 : 1 molar ratios of Co/Ce are hard ferromagnetics. As a result, changing the molar ratio of CeO$_2$ in the sample at the synthesis process leads to changes in the coercive field. A smaller coercivity force is indicative of smaller sizes of nanocatalyst particles.[18]

Also, in this work the residual magnetization ratio ($R = M_r/M_s$) with decreasing cobalt and cerium molar ratios increases from 0.315 until 0.263–0.246. The value of $R > 0.5$ indicates that materials are single domain and $R < 0.5$ relates to multidomain structures.

3.2. Fischer–Tropsch synthesis performance

Iron–cobalt–cerium three-metals nanocatalysts were synthesized using a solvothermal method and the catalytic performance on Fischer–Tropsch synthesis under the operating conditions of (H$_2$/CO = 1, GHSV = 3600 h^{-1}, P = 2 bar) was illustrated. The effect of various Co/Ce molar ratios (1 : 1, 1/2 : 1, 1/4 : 1, 1 : 1/2, 1 : 1/4) at various ranges of operating temperature (270–400 °C) on the Fischer–Tropsch synthesis was investigated (Tables S$_4$–S$_8$†).

3.2.1. Effect of CeO$_2$ as a promoter on transition metals. The purpose of adding oxide promoters like CeO$_2$ is to improve the activity and hydrocarbon selectivity of FT catalyst. The effect of ceria is worth studying because of some controversies about its role. In addition, the reduction of ceria as a promoter can cover the surface-active area of the catalyst and thus lead to a decrease the adsorption capacity of chemisorption. In this case, the cerium role results in changing the hydrocarbon distribution, reducing the catalytic activity and decreasing the olefin selectivity. Another role of CeO$_2$ can be explained in two ways. The first way is it increases the dispersion, stabilization and reducibility of transition metals, which results in a high activity. Also, it decreases the formation of barely reducible mixed oxides. The second way is to provide the facility of CO adsorption and enhance the CO dissociation rate by increasing the strength of the M–C and weakening the C–O bonds.
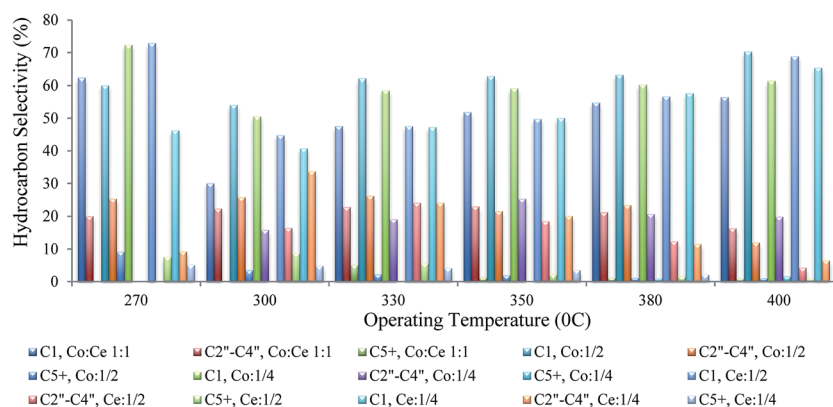

Fig. 12 Hydrocarbon selectivity of iron–cobalt–cerium three-metal nanocatalysts with various Co/Ce molar ratios at different operating temperature ranges.

Actually, CO is bound to metal atoms by its carbon and also to the Ce cations by its oxygen. When ceria exists as Ce(III) cations, it can improve the dissociation of CO by rapid oxidation to Ce(IV) and quickly capture the oxygen atom of CO. These results can be interpreted in terms of the basic property of promoters to electron donate to the metal and back donate electrons from d-orbitals of metal to the CO π^* anti-bonding molecular orbital. In fact, by changing the thermodynamic and kinetic features of adsorbed species (CO and H_2) on active sites, ceria influences surface coverage and reactivity. The better ability of CO dissociation than H_2 and increasing the C*/H* ratios on the catalyst surface leads to a lower hydrogenation activity of the surface carbon species. Therefore, it causes a higher olefin content, higher heavier hydrocarbons and a lower selectivity to methane.

3.2.2. Effect of Co/Ce molar ratio and operating temperature on product selectivity. The activity and selectivity of iron–cobalt–cerium three-metal nanocatalysts to give C''_2–C''_4 light olefins as well as CO conversion are influenced by many factors, which include the nature and interaction effects of iron and cobalt catalysts, the effect of CeO_2 as a controversial promoter, operating conditions, such as temperature, pressure, space velocity, H_2/CO gas feed, *etc.*[19] Iron catalysts indicate a much higher activity for the WGS reaction and compete with the FT reaction at higher CO conversion, which is useful for syngas derived from coal or biomass with lower H_2/CO ratios. A big challenge still for iron catalysts is rapid deactivation. In addition, through iron catalysts, linear alkanes, alkenes and oxygenated products can be obtained. Also, it is reported that the olefin/paraffin ratio is affected by operating conditions, where a higher temperature, space velocity, H_2/CO feed gas and a lower pressure are preferred for olefin formation and a higher olefin/paraffin ratio.[20]

The cobalt catalyst is a priority catalyst for a higher selectivity for the production of long chain paraffins, and has the features of high activity, low WGS activity and a high resistance to deactivation by water.

Since the Fischer–Tropsch synthesis is complicated and hard work, various factors affect product selectivity. In this study, we made a great deal of effort to prepare a large number of Fe–Co–Ce three-metal nanocatalysts with various molar ratios and investigate them for the FT reaction. Therefore, we just report a variety of repeatability molar ratios (Fig. 12). In order to explain the obtained results of changing the Co/Ce molar ratios in the FT synthesis performance, it should be noted that the product selectivity of FT reaction varies with multiple effects concerning each metal singly (iron, cobalt, cerium) as well as the interaction effects of metals on each other. According to the reported different molar ratios of these metals, the optimal condition can be obtained partly for a specific production. Here, the optimal conditions for the specific production of light olefins C''_2–C''_4 at a particular temperature and Co/Ce molar ratio were obtained as 300 °C and 1/1/4, respectively. In summary, at this optimal molar ratio and specific operating temperature, cerium as a promoter performed a positive effect to produce more light olefins by a quick dissociation of CO and higher C*/H* active species on the surface of the catalyst. Also, the results show that the maximum total selectivity towards light olefins obtained for 1/2 : 1 molar ratio of Co/Ce.

To compare with other research on catalyst selectivity, Feyzi *et al.*[21] reported a nano Co/Fe catalyst with 80/20 molar ratios supported on TiO_2–SiO_2 prepared by a sol–gel method in a fixed-bed reactor. The result indicated an optimal light olefin selectivity of 24.5% for C_2–C_3 at a CO conversion of 49.4%. Also, Mirzaei *et al.*[9] studied the effect of operating conditions on cobalt cerium oxide catalysts. The results showed that the catalyst with 80% Co, 20% Ce at an operating temperature of 450 °C performed optimally for light olefin selectivity.

In general as expected, the CO conversion has an increasing trend with enhancing the operating temperature. In the present study, the CO conversion changes from the highest amount to the lowest amount at the beginning of increasing the operating temperature. After this sharp decline in CO conversion, with a further rise in the operating temperature the CO conversion increases (Fig. 13). When the steady state was achieved before an increase in temperature, just in the transition from 270 to 300 °C, therefore, an important deactivation process occurred. These results are due to the fact that the nanocatalyst being used doesn't have a base and, despite a high catalyst activity, the time of deactivation is short. Therefore, by identifying the nanocatalyst feature, the results obtained are explained. The deactivation process is due to two reasons; first, the initial carbon deposition, verified based on XRD peaks of Fe_3C and FeC, is relevant to the catalyst used and also, second, the fast resizing of the nanoparticles at the beginning of reaction, which is interpreted in terms of being placed under operating conditions that result in partly changing the particle size of the fresh nanocatalyst at the initial deactivation stage. These results were verified by XRD with the particle size related to the used catalyst of 62.6 nm. Since the reaction rate is a function of temperature, the partial pressure of gases (monoxide and hydrogen) and catalyst activity, as the initial operating temperature increased to the point of a sharp reduction in CO conversion, the speed of the catalyst deactivation is more effective than the thermal effect. So, from that point of sharp decline, the effect of a temperature rise on the reaction rate surpasses the catalyst deactivation effect. Therefore, the degree of conversion increases with increasing temperature.

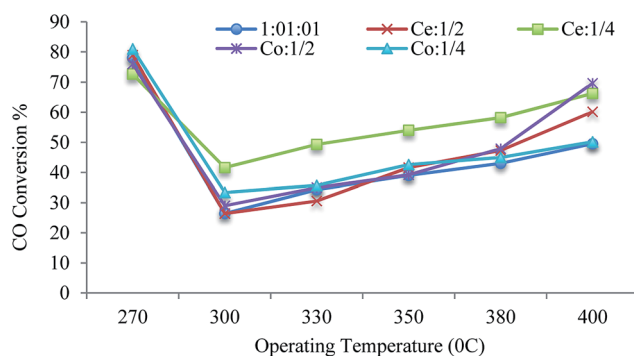The reaction rate of CO conversion is defined as a function of the following parameters:

Fig. 13 Operating temperature *versus* CO conversion of iron–cobalt–cerium three-metal nanocatalysts with different Co/Ce molar ratios.

$$-R_{CO} = Kf(T, P_{CO}, P_{H_2}, \ldots, a) \qquad (3)$$

K: is a constant factor, T: is the operating temperature, P_{CO}: is the partial pressure of CO in the reactor, P_{H_2}: is the partial pressure of H_2 in the reactor, and a: is the catalyst activity at the age of t.

As a conclusion, the selectivity of the nanocatalysts (at constant pressure at different operating temperatures) is influenced by two factors, the catalyst deactivation and thermal effect.

E.g. for a nanocatalyst with a $1:1:1/4$ molar ratio of Fe : Co : Ce, the CO conversion from a high value at 270 °C declines drastically at 300 °C due to a more significant catalyst deactivation effect. After that, with increasing the operating temperature from 330 °C to 400 °C, the CO conversion enhances as a result of more prominent thermal effects.

4. Conclusion

A variety of preparation and operating conditions that influence catalytic performance and selectivity were studied. Iron–cobalt–cerium three-metal nanocatalysts of various cobalt and cerium molar ratios were synthesized by a solvothermal method. The results showed that the optimal Co/Ce molar ratio and operating temperature for light olefin (C''_2–C''_4) selectivity was achieved at $1:1/4$ and 300 °C. The characterization of nanocatalysts was performed by SEM, EDX, XRD, FTIR, TPR and VSM techniques. From the FTIR spectra it was concluded that oleylamine surrounded the surface of the nanocatalyst. The XRD spectra and EDS data confirmed the formation of oxidic phases of the nanocatalysts. The results indicate that with decreasing cobalt and cerium molar ratios, the particle size enhances. Comparing SEM and XRD data demonstrated the larger particle size because of agglomeration. From the TPR, it was observed that the reduction peaks of nanocatalysts with decreasing cobalt and cerium molar ratios reduced at higher temperatures. The magnetic properties are also influenced by the cobalt and cerium molar ratios and the synthesized samples indicate a ferromagnetic behavior. The VSM measurement of nanocatalysts exhibits that the saturation magnetization, coercivity and residual magnetization are dependent on particle size and increase by reducing the amount of cobalt and cerium.

Acknowledgements

References

1 S. Sartipi, K. Parashar, M. Makkee, J. Gascon and F. Kapteijn, Breaking the Fischer–Tropsch synthesis selectivity: direct conversion of syngas to gasoline over hierarchical Co/H-ZSM-5 catalysts, *Catal. Sci. Technol.*, 2013, 572.

2 O. O. James, B. Chowdhury, M. Adediran Mesubi and S. Maity, Reflections on the chemistry of the Fischer–Tropsch synthesis, *RSC Adv.*, 2012, 7347.

3 J. Wang, H. Li, D. Li, J. P. den Breejen and B. Hou, Influence of the bimodal pore structure on the CO hydrogenation activity and selectivity of cobalt catalysts, *RSC Adv.*, 2015, 65358.

4 M. E. Dry, The Fischer–Tropsch process, *Catal Today*, 2002, 227.

5 M. E. Dry, Practical and theoretical aspects of the catalytic Fischer–Tropsch process, *Appl. Catal., A*, 1996, 319.

6 Y. Liu, J.-F. Chen and Y. Zhang, The effect of pore size or iron particle size on the formation of light olefins in Fischer–Tropsch synthesis, *RSC Adv.*, 2015, 29002.

7 D. B. Bukur, B. Todic and N. Elbashir, Role of water–gas-shift reaction in Fischer–Tropsch synthesis on iron catalysts, *Catal. Today*, 2015, 66.

8 J. Gao, Q. Liu, F. Gu, B. Liu, Z. Zhong and F. Su, Recent advances in methanation catalysts for the production of synthetic natural gas, *RSC Adv.*, 2015, 22759.

9 A. A. Mirzaei, M. Galavy, A. Beigbabaei and V. Eslamimanesh, Preparation and operation conditions for cobalt cerium oxide catalysts used in the conversion of synthesis gas into light olefins, *J. Iran. Chem. Soc.*, 2007, 347.

10 M. Arsalanfar, A. A. Mirzaei, H. R. Bozorgzadeh and H. Atashi, Effect of process conditions on the surface reaction rates and catalytic performance of MgO supported Fe–Co–Mn catalyst for CO Hydrogenation, *J. Ind. Eng. Chem.*, 2012, 2092.

11 Y. P. Li, T. J. Wang, C. Z. Wu, X. X. Qin and N. Tsubaki, Effect of Ru addition to Co/SiO₂/HZSM-5 catalysts on Fischer–Tropsch synthesis of gasoline range hydrocarbons, *Catal. Commun.*, 2009, 1868.

12 M. L. DosSantos, R. C. Lima, C. S. Riccardi, R. L. Tranquilin, P. R. Bueno, J. A. Varela and E. Longo, Preparation and characterization of ceria nanospheres by microwave-hydrothermal method, *Mater. Lett.*, 2008, 4509.

13 H. Su, S. Zeng, H. Dong, Y. Du, Y. Zhang and R. Hu, Pillared Montmorillonite Supported Cobalt Catalysts for the Fischer–Tropsch Reaction, *Appl. Clay Sci.*, 2009, 325.

14 K. J. Davies, S. Wells and S. W. Charles, The effect of temperature and oleate adsorption on the growth of maghemite particles, *J. Magn. Magn. Mater.*, 1993, 24.

15 B. De Rivas, J. Gutierrez-Ortiz, R. Lopez-Fonseca and J. Gonzalez-Velasco, Analysis of the simultaneous catalytic combustion of chlorinated aliphatic pollutants and toluene over ceria–zirconia mixed oxides, *Appl. Catal., A*, 2006, 54.

16 Y. Köseoğlu, F. Alan, M. Tan, R. Yilgin and M. Öztürk, Low temperature hydrothermal synthesis and characterization of Mn doped cobalt ferrite nanoparticles, *Ceram. Int.*, 2012, 3625.

17 C. Luo, Y. Fu, D. Zhang, S. Yuan, Y. Zhai, S. Dong and H. Zhai, Temperature dependent coercivity and magnetization of light rare-earth Nd doped permalloy thin films, *J. Magn. Magn. Mater.*, 2015, 711.

18 P. A. Chernavskii, A. Y. Khodakov, G. V. Pankina, J.-S. Girardon and E. Quinet, *In situ* characterization of the

genesis of cobalt metal particles in silica-supported Fischer–Tropsch catalysts using Foner magnetic method, *Appl. Catal., A*, 2006, 108.

19 Y. L. Yao, X. Y. Liu, D. Hildebrandt and D. Glasser, Fischer–Tropsch synthesis using $H_2/CO/CO_2$ syngas mixture: A comparison of paraffin to olefin ratios for iron and cobalt based catalysts, *Appl. Catal., A*, 2012, 433.

20 F. Yan, W. Qian, Q. Sun, H. Zhang, W. Ying and D. Fang, Product distributions and olefin-to-paraffin ratio over an iron-based catalyst for Fischer–Tropsch synthesis, *React. Kinet., Mech. Catal.*, 2014, 471.

21 M. Feyzi, N. Yaghobi and V. Eslamimanesh, Cobalt–iron nano catalysts supported on TiO_2–SiO_2: characterization and catalytic performance in Fischer-Tropsch synthesis, *Mater. Res. Bull.*, 2015, **72**, 143–153.